Carbohydrate Polymers 77 (2009) 306–315

Contents lists available at ScienceDirect

Carbohydrate Polymers

journal homepage: www.elsevier.com/locate/carbpol

Investigation of alginate gel inhomogeneity in simulated gastro-intestinal conditions using magnetic resonance imaging and transmission electron microscopy

Peter J. Wright [a], Elisabetta Ciampi [b], Caroline L. Hoad [a], Anthony C. Weaver [b], Michael van Ginkel [b], Luca Marciani [a], Penny Gowland [a], Michael F. Butler [c], Phillippa Rayment [c,*]

[a] Sir Peter Mansfield Magnetic Resonance Centre, University of Nottingham, University Park, Nottingham NG7 2RD, UK
[b] Measurement Science, Unilever R&D Colworth, Sharnbrook, Bedfordshire MK44 1LQ, UK
[c] Corporate Research, Unilever R&D Colworth, Sharnbrook, Bedfordshire MK44 1LQ, UK

ARTICLE INFO

Article history:
Received 16 October 2008
Received in revised form 1 December 2008
Accepted 23 December 2008
Available online 14 January 2009

Keywords:
Alginate
Gel
Inhomogeneity
Microstructure
Magnetic resonance imaging (MRI)
Porosity
T_2
Transmission electron microscopy (TEM)
Watershed transformation

ABSTRACT

The inhomogeneity of alginate gel beads prepared by an external diffusion method has been characterised using spatially resolved nuclear magnetic resonance or "magnetic resonance imaging" (MRI) and transmission electron microscopy (TEM). The beads exhibited various degrees of inhomogeneity although reducing the length of exposure to the gelling bath and the presence of non-gelling ions decreased gel inhomogeneity. In order to gain information regarding the gastro-intestinal functionality of these beads for *in vivo* applications, they were exposed to simulated gastro-intestinal conditions. The increased polymer concentration at the edge of the beads was shown to persist throughout our gastro-intestinal model despite the centre of the bead becoming progressively more porous in nature. The porosity of the alginate gels has been quantified by image analysis of transmission electron micrographs and shown to depend on both location within the bead and gastro-intestinal conditions. We suggest that such changes in porosity of these alginate beads during simulated gastro-intestinal conditions may make these an attractive option for controlled delivery applications *in vivo*.

1. Introduction

Alginates are natural polysaccharides mainly isolated from various species of brown algae where their biological function is to provide both strength and flexibility to the cellular tissue. They are used in a wide range of applications particularly in the food and pharmaceutical industry due to their capacity to hold water, form gels and stabilise emulsions. Alginates are unbranched block co-polymers of (1 → 4)-linked residues of β-D-mannuronic (M) acid and α-L-guluronic (G) acid. The ion-binding properties of alginates are the basis for their gelling properties and have been the subject of much research interest (Emmerichs, Wingender, Flemming, & Mayer, 2004; Haug, 1961; Haug & Smidsrød, 1970; Ouwerx, Velings, Mestdaugh, & Axelos, 1998; Smidsrød, 1974). Gel formation occurs due to an ionic interaction between G residues from 2 or more alginate chains and multivalent cations, typically calcium (Ca^{2+}), to form a three-dimensional network, well described by an "egg-box model" (Grant, Morris, Rees, Smith, & Thom, 1973). Alginates, particularly with high G content, are also extensively used as an immobilisation matrix in encapsulation applications due to their good biocompatibility (Green et al., 2005; Mørch, Donati, Strand, & Skjåk-Bræk, 2006; Skjåk-Bræk & Espevik, 1996; Thu et al., 1996). More recently the potential for alginates in polymer-controlled drug delivery applications has been highlighted (Peppas, 2004; Tønnesen & Karlsen, 2002).

This study is concerned with the investigation of calcium alginate beads, prepared using different conditions of exposure to a calcium chloride gelling bath and the effect that simulated gastro-intestinal (GI) conditions have on the gel microstructure and homogeneity. It is well known that alginate gels prepared by external (dialysis) methods often exhibit a heterogeneous concentration distribution (Smidsrød & Draget, 1996). However, the effect this has on alginate pore size distribution, particularly in simulated GI conditions, is poorly understood. The use of such materials as physiologically responsive hydrogels is dependent on the swelling behaviour of the polymer in GI conditions (Peppas, 2004). We have previously shown that alginate beads shrink in gastric conditions and swell in intestinal conditions due to changes in electrostatic forces brought about by adjusting pH and ionic strength conditions (Rayment et al., 2009). However, in this paper, we utilise spatially resolved NMR (MRI) and TEM to characterise alginate gel networks formed under different conditions to further understand this effect. It has been previously reported that, for dilute polysaccharides

* Corresponding author. Tel.: +44 1234 222769; fax: +44 1234 248010.
E-mail address: pip.rayment@unilever.com (P. Rayment).

0144-8617/$ - see front matter © 2009 Elsevier Ltd. All rights reserved.
doi:10.1016/j.carbpol.2008.12.025

solutions and gels, the NMR signal arising from the water proton is modulated by exchange between the water protons and protons of macromolecules (polysaccharide chain) (Hills, Cano, & Belton, 1991; Potter, Carpenter, & Hall, 1993). The observed NMR relaxation time, T_2, is a complex function of the number of exchangeable protons on the polysaccharide, the rate of exchange with those sites and the relaxation times of the protons at the exchange sites. NMR transverse relaxation times (T_2) of water protons in polysaccharide gels are considerably decreased compared to bulk water values (Ablett, Lillford, Baghdadi, & Derbyshire, 1976) due to the reduced flexibility of the polymer chains. The state of aggregation and gelation of the polysaccharide determines the extent of this reduction. Therefore T_2 relaxation is a sensitive indicator of the state of gelation and a powerful tool for characterisation of microstructural properties in gels.

This paper describes the effect that both preparation conditions and simulated GI conditions have on alginate gel microstructure and homogeneity using MRI and TEM. Furthermore, we have utilised MR imaging techniques at two different field strengths. This has allowed us to access both high spatial resolution microstructural information at 7 T, as well as probe dynamic microstructural changes at lower field strengths (3 T), which may be utilised *in vivo*. Previous work has highlighted the potential to correlate *in vitro* MRI measurements using a whole-body MRI scanner at 3T with investigation of such systems *in situ* during GI transit (Hoad et al., 2009; Rayment et al., 2009).

2. Materials and methods

2.1. Materials

Sodium alginate (Manugel DMB™) was obtained from ISP Alginates (Tadworth, UK). The average molecular weight of the alginate was determined to be 2.83×10^5 Da using HPSEC-MALLS and the guluronic acid residue content was determined as 72% using ^{1}H NMR analysis. Analytical grade calcium (II) chloride (C3881) was obtained from Sigma–Aldrich (UK) and sodium chloride (S/3160/63) was obtained from Fisher Scientific (UK).

2.2. Preparation of calcium alginate beads

A 1.5% (w/w) sodium alginate solution was prepared by gradually sprinkling the biopolymer powder into deionised water whilst stirring at 22 °C. The solution was stirred for approximately 2 h to ensure complete hydration.

Two types of calcium alginate beads were prepared dependant on the length of time the beads were exposed to calcium chloride. "Strong" (strongly gelled) beads were prepared by dripping 100 ml of 1.5% alginate solution into 400 ml of 0.025 M calcium chloride solution using a 250 ml funnel and 200 μl Gilson tip cut to 39 mm to increase the drip rate. The Gilson tip was held in place using parafilm. Once all the alginate solution had dripped into the calcium chloride solution, the beads were sieved and rinsed in fresh calcium chloride solution after 5 min. The beads were placed into a storage container with 400 ml fresh calcium chloride solution (control solution) and stored at 5 °C for 22 h before characterisation. Weak (weakly gelled) beads were prepared by dripping 100 ml of 1.5% alginate solution into 400 ml of 0.025 M calcium chloride solution for 2 min. The alginate beads remained in the calcium chloride solution for a further 3 min with gentle stirring before being sieved and rinsed with 0.05 M sodium chloride solution. Finally the beads were stored in 400 ml fresh sodium chloride solution (control solution) at 5 °C for 22 h before characterisation. Following storage, the bead diameter was determined as described in Rayment et al. (2009). The strong beads were smaller (approximately 3.9 mm) compared to the weak beads (approximately 4.3 mm) reflecting an increased syneresis of the gel at high calcium concentrations (Kim, 1990; Martinsen, Skjåk-Bræk, & Smidsrød, 1989).

2.3. Protocol for simulating gastric and intestinal conditions

Solutions were prepared to be physiologically similar to gastric and intestinal juices for a fasted human (Altman, 1961). The beads were exposed to simulated gastric conditions (2.86 g/L NaCl, 0.865 g/L KCl and 0.4 g/L $CaCl_2$; all Sigma–Aldrich Analytical Grade Chemicals) for 2 h at 37 °C. The pH of the gastric solution was reduced to pH 2.0 using 4 M HCl (Fluka 84435) after 15 min to simulate *in vivo* acidification. The beads were then exposed to simulated intestinal conditions (6.5 g/L NaCl, 0.835 g/L KCl, 0.22 g/L $CaCl_2$ and 1.386 g/L $NaHCO_3$) for 3 h. These experiments were conducted using a simulated intestinal solution containing simple salts and a pH close to that found in parts of the human intestine. Bile extract was not included in these studies and we expect the gel integrity to be further weakened by their inclusion. This is investigated in future studies. The final pH of the intestinal phase solution was approximately 8.0. Both solutions were made 24 h before an experiment.

2.4. ^{1}H MRI at 7 T for high resolution imaging of beads

^{1}H 2D NMR images were recorded on a Bruker DSX 300 spectrometer (operating at a proton frequency of 300 MHz) with a Bruker Avance console and equipped with a standard micro-imaging Micro 2.5 probehead and a 15 mm RF birdcage resonator.

One or more alginate gel beads of the same type were analysed simultaneously while immersed in the appropriate solution. In a typical experiment, the alginate beads were placed in an NMR tube horizontal slice images through the centre of the beads were obtained using a standard single spin–echo imaging sequence. The slice thickness was 1 mm; field of view was 15×15 mm^2; and in-plane voxel resolution was 59×59 μm^2. The recycle time was 10 s and the echo time (*TE*) was typically 40 ms with total scan time lasting approximately 42 min.

For spatially resolved measurements of the transverse relaxation time T_2 of the water protons within the gel, separate images were acquired at 24 echo times (*TE* = 10–240 ms in steps of 10 ms). All other imaging sequence parameters remained constant between images. The maps of initial magnetisation M_0 and of relaxation time T_2 were obtained by fitting a single exponential function to the signal decay M of each pixel, $M = M_0 \exp(-TE/T_2)$ + constant. Radial averages of M_0 and T_2 for each bead were extracted by averaging the corresponding maps in 'shells' from the centre of the bead towards the surface.

Strong and weak alginate beads were exposed to solutions simulating gastric and intestinal conditions as described previously. An individual bead was followed throughout the experiment, separated from the others using a small sieve. It was scanned at the end of each phase of exposure (i.e. control, gastric and intestinal conditions), when it was removed from the main sample and immersed in a small quantity of appropriate solution.

Profiles across the images of the beads were made by radial averaging, so that each point on the profile was obtained by averaging the signal in the map in 'shells' from the centre of the strong bead towards the surface.

2.5. Magnetic resonance imaging (MRI) at 3 T

Data were acquired on a 3.0 T Philips Achieva (Philips Medical Systems) whole body scanner with an eight element SENSE-Head coil. A T_2-weighted high resolution Turbo Spin Echo (TSE) sequence

was used to scan the beads with 150 mm field of view (FOV) which was 60% rectangular; 512 × 512 matrix giving 0.29 × 0.29 mm^2 in-plane resolution; 1 mm slice thickness; 15 ms TSE echo spacing and an echo train length of 18. The sequence created double echo images with echo times TE_1 = 45 ms and TE_2 = 240 ms; repetition time (TR) = 3000 ms; number of averages = 4 and bandwidth/pixel = 138 Hz. Beads were left in the appropriate solutions in the scanner for the duration of the experiments and scanned approximately every 30 min.

T_2 maps were generated from the two echoes using the following equation:

$$T_2(i,j) = \frac{TE_2 - TE_1}{\ln(S(TE_1(i,j))) - \ln(S(TE_2(i,j)))}$$

where $S(TE_1(i,j))$ and $S(TE_2(i,j))$ are the signal intensity levels at matrix position (i,j) for the first and second echo data, respectively. This simple 2 point method for estimating T_2 (Deichmann et al., 1995; McKenzie, Chen, Drost, & Prato, 1999; Tyler, Moore, Marciani, & Gowland, 2004) was used allowing for multiple measurements in both gastric and intestinal solutions to provide high spatial resolution in a reasonable imaging time (<10 min per scan) using the whole body scanner. T_2 values are expected to be higher at 3 T compared to 7 T.

Strong and weak alginate beads were exposed to a series of solutions designed to simulate GI conditions as described above. T_2 measurements were performed approximately every 30 min for 5 h (2 h in gastric solution and 3 h in intestinal solution).

Line profiles through the beads were measured using a graphical user interface written in IDL® (Research Systems, Boulder, Colorado, USA). The user defined the centre of a vertical or horizontal line profile through the bead of interest and the profile was saved. The same bead was tracked within each solution, although different beads were studied in each phase of the gastro-intestinal simulation.

2.6. Transmission electron microscopy (TEM) and image analysis

Strong alginate beads were examined at the end of the gastric and intestinal phases of the experiment as well as alginate beads stored in the control solution. Due to the liquid nature of the centre of the weak beads, the gel microstructure could not be investigated using this technique.

To enhance fixation, the beads were cut in half and then placed in 0.1% aq. ruthenium tetroxide for 90 min. The beads were then rinsed using distilled water for 20 min and the process repeated. The beads were stained in 1% aq. uranyl acetate overnight, dehydrated in ethanol and infiltrated with epoxy resin, which was polymerised at 60 °C for 48 h. Sections of approximately 100 nm thickness were prepared and stained in lead citrate. The sections were then examined using a Jeol 1200 TEM at 100 kV at different positions across the microstructure. Fig. 1 shows the areas of the gel microstructure examined: edge of bead (E), halfway towards the centre of the bead (I) and the centre of the bead (C).

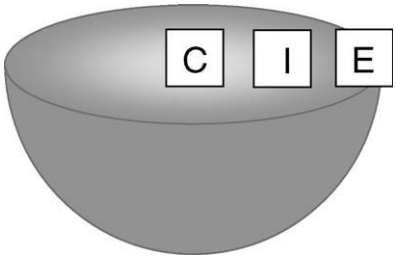

Fig. 1. Schematic of strong alginate bead depicting areas of gel microstructure examined by transmission electron microscopy: edge of bead (E), halfway inside bead (I) and centre of bead (C).

In addition to our visual interpretation, we have quantified the gel pore structure using image analysis and an apparent pore size distribution was determined using a watershed transformation (Soille, 1999). The segmentation is based on interpretation of an image as a height map where the dark polymer rich regions are described as 'dams', the bright polymer poor areas are 'catchment basins' and analysis of 'flooding' of the image with water is undertaken. The watershed divides an image into regions corresponding to the underlying intensity structure, separated by one-pixel thick borders.

The algorithm is comprised of two steps (Fig. 2), where Step 2 is repeated:

1. Each local intensity maximum is the origin of a region (initialisation).
2. Of all the pixels not yet classified and bordering a region, the algorithm takes the brightest pixel. If this pixel borders a single region it is classified as part of that region otherwise it is classified as a boundary pixel.

However, since each pore can contain multiple local intensity maxima, the watershed algorithm tends to subdivide pores. To prevent this, a Gaussian pre-smoothing is used. In addition, the watershed implementation of DIPimage (Luengo Hendriks, Rieger, van Ginkel, van Kempen, & L. J., 1999) allows us to apply an intensity contrast criterion to each region as it is growing. If two regions

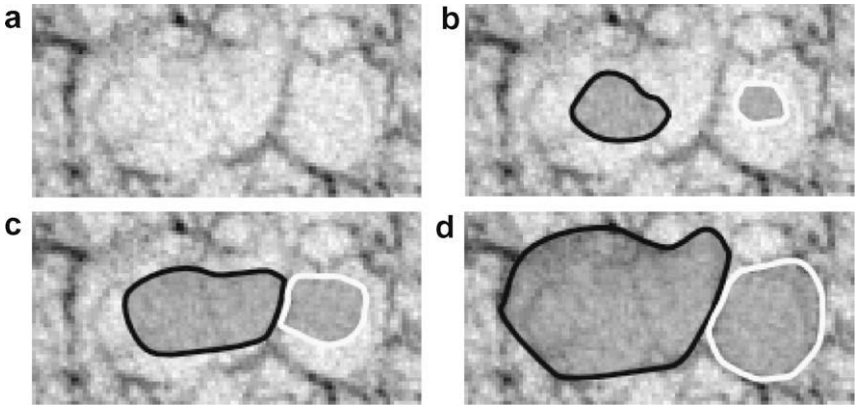

Fig. 2. (a) Original image. (b) Two regions are followed as they grow. (c) The two regions have grown to the point where they have met and started to grow along the line separating them. (d) All pixels of the two regions have been classified.

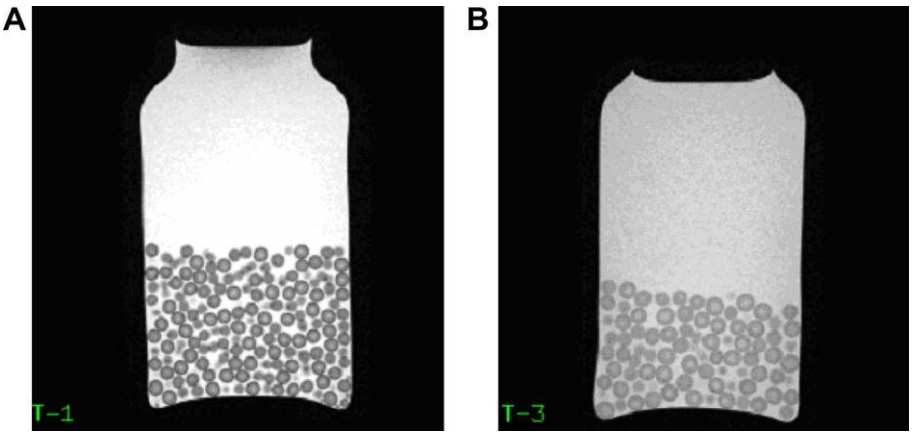

Fig. 3. T_2-weighted high resolution images of (A) strong alginate beads in calcium chloride solution and (B) weak alginate beads in sodium chloride solution. Both images were obtained using a 3.0 T Intera Achieva (Philips Medical Systems) MRI scanner.

that do not achieve this criterion meet during the growth phase, they are merged.

The results are presented as cumulative, area-weighted, distributions. These distributions give the area fraction of the sample that is covered by pores up to a given area. This pore area is parameterised using the equivalent diameter d, which corresponds to an equivalent area

$$A_e(d) = \frac{1}{4}\pi d^2,$$

If the area of the ith pore is A_i, then the cumulative, area-weighted, distribution $C(d)$ is computed as:

$$C(d) = \sum_{A_i<A_e(d)} A_i \Big/ \sum_{all} A_i$$

3. Results

Fig. 3 shows a typical T_2-weighted image of strong (A) and weak (B) alginate beads at 3 T in a container of calcium chloride control solution and sodium chloride solution, respectively. These MR images are generated from the protons of water molecules where bulk water appears bright and water in the gel appears darker. It is clear from these images that the intensity is different for each bead type and is not constant across the beads. This is depicted by the beads appearing darker at the edge than the centre.

This observed gel heterogeneity was examined further at a higher magnetic field strength. Fig. 4 shows MR images of strong and weak beads at 7 T. Again, it is clear that the gel beads are not homogeneous from the edge of the bead to the centre. For the strong alginate beads in particular (Fig. 4A), the intensity of the NMR signal in the T_2-weighted image is not constant across the beads, rather the NMR intensity is lower at the bead edge than at the centre. For the weak alginate beads, the intensity of the T_2-weighted image is higher and there is little visual intensity gradient across this system.

It is also observed that the weak alginate beads are bigger than the strong alginate beads which is discussed in our previous publication (Rayment et al., 2009).

Fig. 5 displays our results of a more detailed investigation of the alginate beads in simulated GI conditions using MRI at 7 T. Fig. 5a and b show our results for the strong and weak alginate beads, respectively, in control, gastric and intestinal conditions. In gastric (G) conditions, the strong beads shrink and the intensity of the MR images decreases particularly at the edge of the bead. In intestinal (I) conditions, the strong beads swell and the intensity of the MR images increases and becomes more homogeneous across the bead. Fig. 5a also shows the corresponding proton density (M_0) and T_2 radial averages, where each value is obtained by averaging the corresponding maps in 'shells' from the centre of the strong bead towards the surface. There are no significant differences in the radial proton density average across the strong beads in all conditions. However, T_2 is higher at the centre of the strong beads and lower at the edges in control conditions, ranging from approximately 48–34 ms, and in gastric conditions, ranging from approximately 44–22 ms, respectively. In intestinal conditions, T_2 is homogeneous across the bead (approximately 48 ms). The results

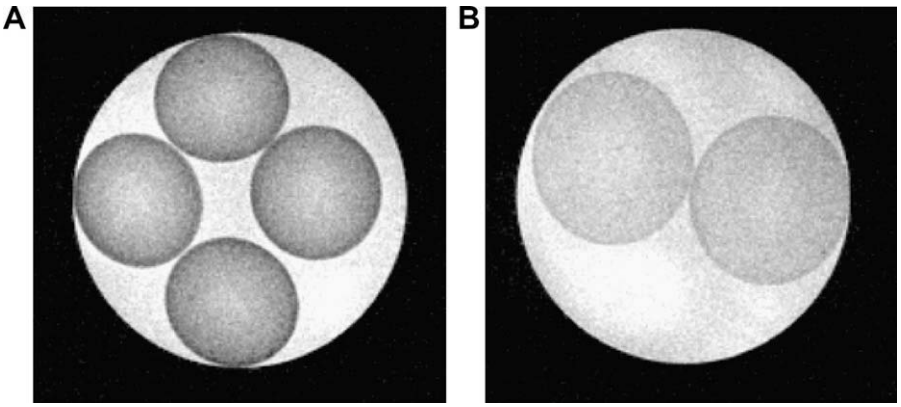

Fig. 4. MR images of strong (A) and weak (B) alginate gel beads at 7 T (TE = 40 ms) in calcium chloride and sodium chloride solution, respectively.

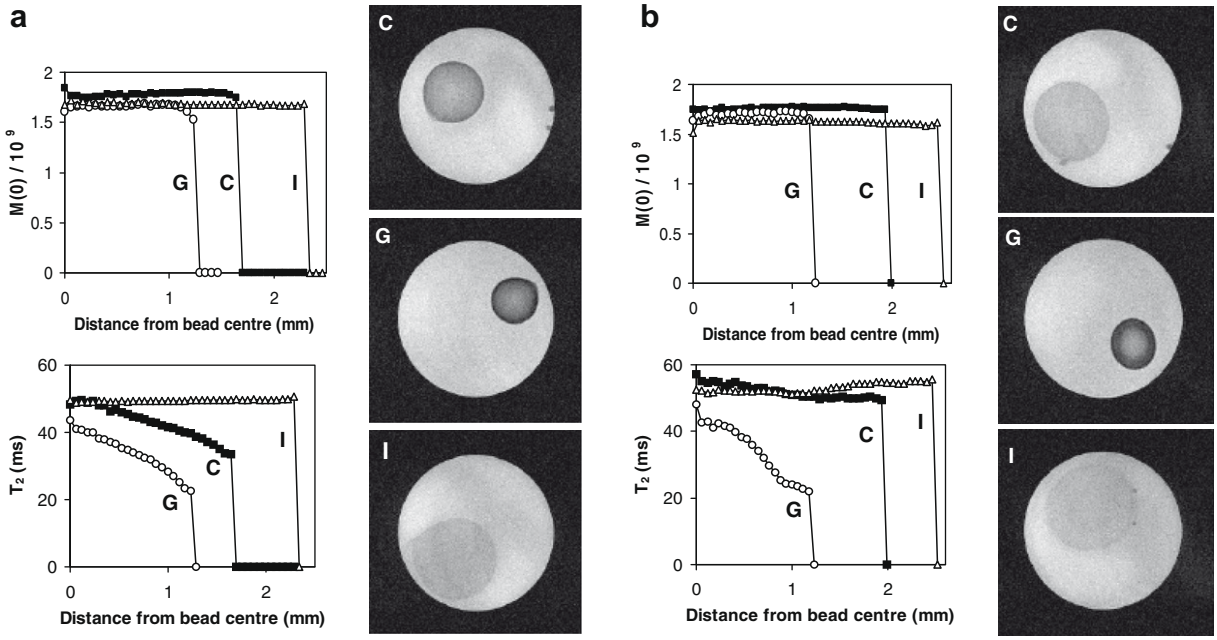

Fig. 5. Plots of radial average of the initial magnetisation, M_0, and of the transverse relaxation time, T_2, through the centre of the bead and MR images in control (C), gastric (G) and intestinal (I) conditions for (a) strong and (b) weak alginate bead. Images were acquired after 130 min in gastric conditions and after 190 (weak) and 200 (strong) min in intestinal solution. Each point in the radial average plots represents the average over all points at that distance from the centre of the bead. The standard deviation of the radial average is within 6% for M_0 and 10% for T_2.

for the weak alginate bead system are displayed in Fig. 5b. Similarly, there is little difference in the radial proton density average across the weak bead in all conditions but T_2 is altered particularly in gastric conditions where it is shorter and more heterogeneous across the bead, ranging from approximately 48 ms at the centre and 22 ms at the outer edge of the bead.

Fig. 6 shows T_2 values across the beads for the strong and weak bead system in control and for various times in gastric and intestinal conditions in the whole-body MRI scanner at 3 T. As expected, the T_2 values are generally higher than those determined at the higher field strength. Fig. 7 shows the change in bead diameter, measured from the 3 T MRI bead profiles, as the beads pass through the simulated gastric and intestinal phases. In agreement with 7 T results (Fig. 5A), in control conditions the strong beads are smaller than the weak beads and the T_2 of the strong beads are shorter than the weak beads with T_2 generally being lower at the edge than at the centre of the beads. The T_2 values range from approximately 180 ms at the centre of the strong beads to 90 ms at the edge compared to 550 ms at the centre and 340 ms at the edge of the weak beads. When placed in gastric conditions the weak beads shrink and the T_2 values shorten to that more similar to the strong beads (approximately 90–200 ms from edge to centre of beads). Less effect is observed for the strong alginate beads with most of the changes appearing to have occurred by the 50 min time point. Since the pH of the gastric solution is reduced after 15 min, shrinkage and a reduction in T_2 is not observed at the 5 min time point. For both bead systems, the gel remains inhomogeneous across the bead with T_2 being shorter at the edge than in the centre. When subsequently placed in intestinal conditions, both types of beads swell and their respective T_2 increase again and show an increased homogeneity across the bead, confirming the 7 T results.

The gel inhomogeneity was also examined by transmission electron microscopy (Fig. 8). For the strong beads, a variation in microstructure between the edge and centre of the bead was observed in all conditions. In general, the gel has a denser, tight network at the edge (Fig. 8A, D and G), and is more open and porous at the centre (Fig. 8C, F and I), which is consistent with the MR T_2 results (Figs. 5 and 6). The gel microstructure forms a denser network in gastric conditions (Fig. 8D, E and F) compared to the control (Fig. 8A–C). In intestinal conditions (Fig. 8G, H and I), the gel microstructure appears to become more open and porous in nature.

Fig. 9 shows the pore size distributions of the gel microstructure from the edge, halfway into, and at the centre of the bead under control conditions. Here, there is no appreciable difference in the pore size at the halfway-in point (I) and that at the centre of the bead (C). However, the pores at the edge of beads are significantly smaller compared to further inside.

Fig. 10 compares the porous gel microstructure at the edge (a), halfway-in (b) and centre (c) of the beads in control, gastric and intestinal conditions. At the edge (a), the pore size distributions under the different conditions are all very similar. At the halfway-in point and at the centre, the pore size distribution under intestinal conditions shows larger pores. At the centre (c), the difference in pore size distribution under control and gastric conditions is small. At the halfway-in point (b), the size distribution under intestinal conditions tapers off slowly at the right hand side of the curve, indicating a relatively greater proportion of larger pores. During the experiments, it emerged that a single setting ($p = 40$) for the contrast parameter p of the watershed algorithm works well with the exception of the structure at the halfway-in and centre under intestinal conditions. For these we have set $p = 50$. Fig. 11 shows the effect of the parameter p.

4. Discussion

We have used MRI and TEM to show that alginate gel beads prepared by an external diffusion method produce inhomogeneous gel networks. This has been previously reported (Smidsrød & Draget, 1996) and is due to the fact that before the alginate is confined within the gel network it can diffuse towards the inwardly moving solvent (calcium chloride) front and therefore form a bead with a higher concentration of alginate at the surface (edge) than in the

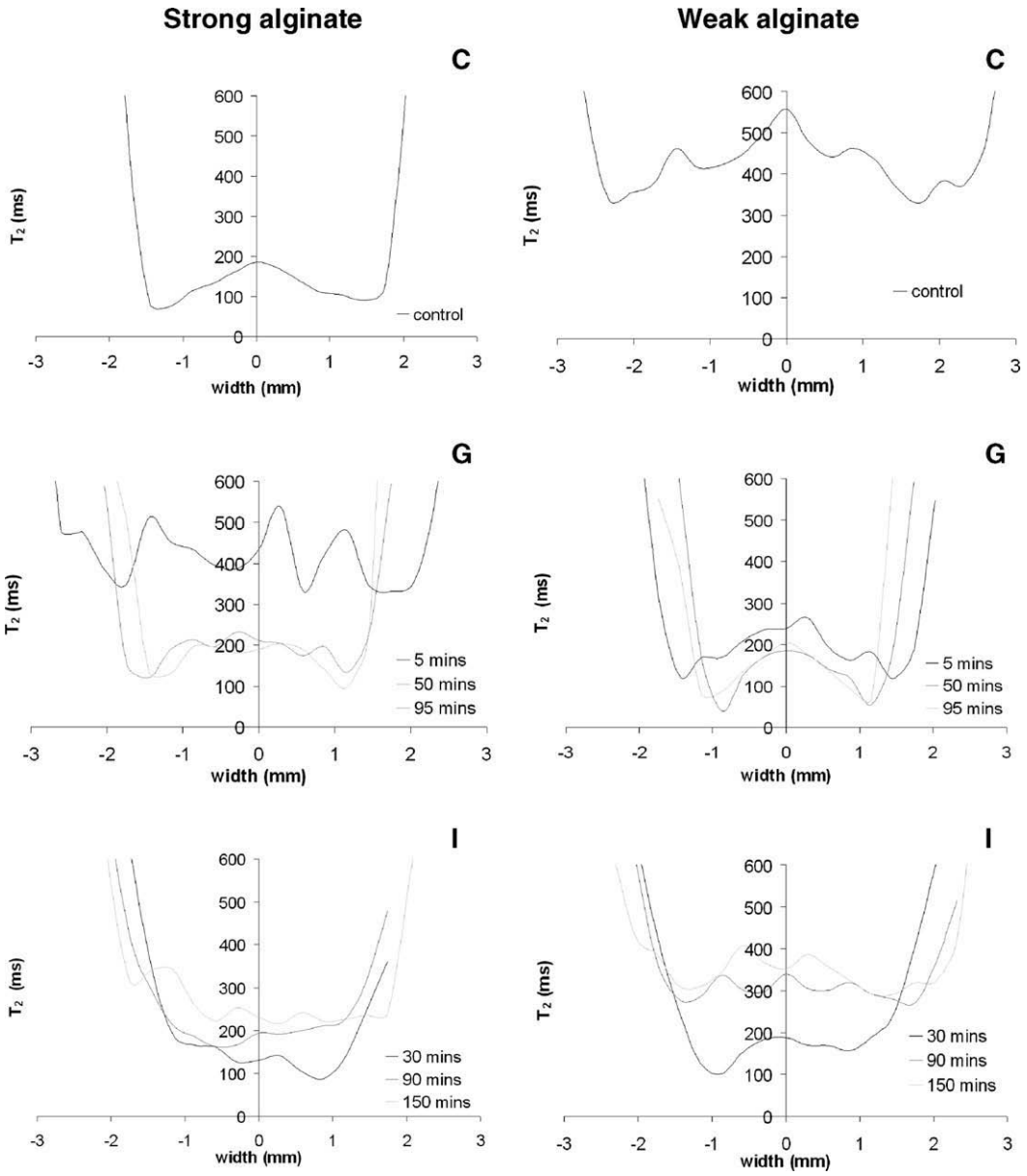

Fig. 6. Gel T_2 profiles at 3 T for strong and weak alginate beads in control (C), gastric (G) and intestinal (I) conditions.

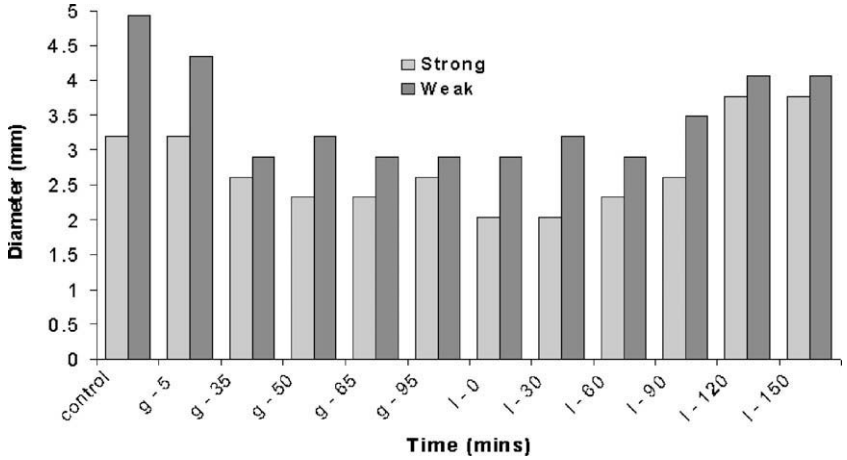

Fig. 7. Evolution of the gel bead diameter measured from the 3 T MRI profiles for bead exposure to control (C), gastric (G) and intestinal (I) solutions.

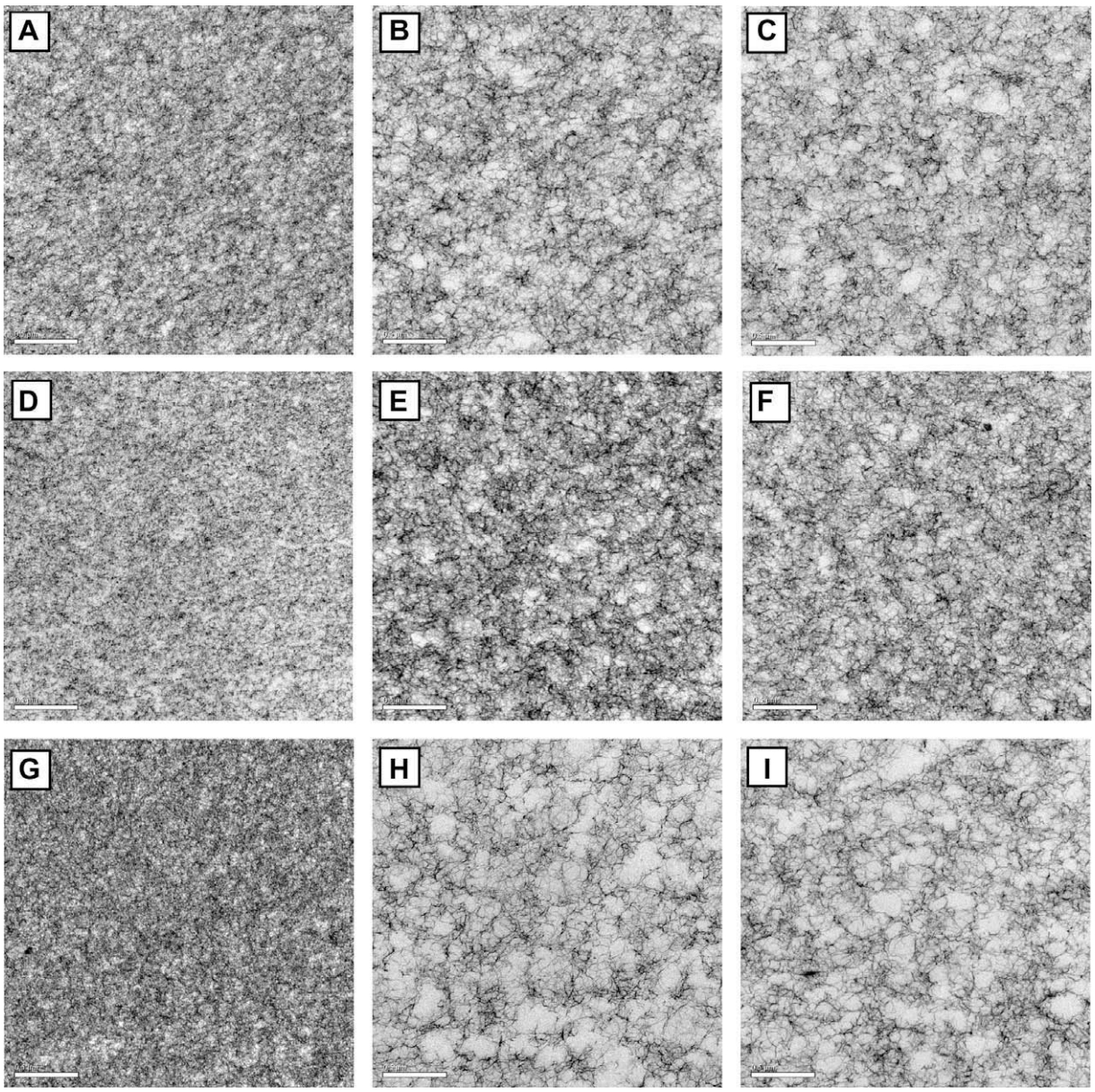

Fig. 8. Transmission electron micrographs of 1.5% strong alginate bead in control and gastro-intestinal conditions. Sample examined at: (A) control (outer edge), (B) control (halfway-in), (C) control (centre), (D) gastric (outer edge), (E) gastric (halfway-in), (F) gastric (centre), (G) intestinal (outer edge), (H) intestinal (halfway-in) and (I) intestinal (centre). Scale bar = 0.5 μm.

centre. In general, low molecular weight alginate, low concentration of gelling (divalent) ions and the absence of non-gelling (monovalent) ions results in highest inhomogeneity (Skjåk-Bræk, Grasdalen, & Smidsrød, 1989; Strand, Mørch, Espevik, & Skjåk-Bræk, 2003). Our strongly gelled bead system showed much greater inhomogeneity compared to the weakly gelled bead system in control conditions, presumably due to the increased exposure to calcium ions and the absence of monovalent ions in this system. Simpson, Grant, Blackband, and Constantinidis (2003) acquired T_2-weighted MR images of alginate beads and showed good radial signal homogeneity across the diameter. This may have been due to the presence of monovalent cations, since the alginate solutions were all prepared in physiological saline (0.85% NaCl) in this case, and also the smaller size of the beads prepared (800–900 μm). Furthermore, in our previous publication (Rayment et al., 2009), we describe the effect of calcium concentration on bead size since the strong beads are smaller in size due to increased syneresis. It is well established that calcium alginate gels shrink during gel formation resulting in a loss of water (syneresis) and an increase in polymer concentration (Smidsrød & Draget, 1996).

We also show that there is little difference in radial proton density across the beads, the majority of the heterogeneity being reflected by the T_2 parameter as described previously. It has been reported that there is little or no contrast from a proton density map (M_0), as the distribution of water in a dilute polysaccharide gel is generally approximately constant (Potter, Herrod, Carpenter, & Hall, 1993). Hence, the variation in image intensity is, to a first approximation, attributed to the variation in T_2 of the water protons.

For both types of alginate bead, T_2 is not constant across the sample. Previous work on dilute neutral alginate systems has experimentally shown that T_2 is inversely proportional to polymer concentration (Duez et al., 2000; Hills et al., 2000; Potter, Carpenter et al., 1993; Thu et al., 2000). Hence T_2 measured in control con-

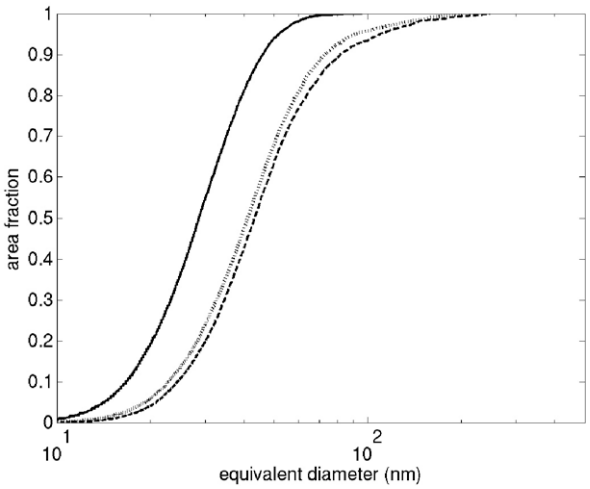

Fig. 9. Watershed analysis of TEMs of strong alginate gel bead in control conditions. Sample examined at outer edge (solid line), halfway-in (dashed line) and centre (dotted line, appears almost grey).

ditions can be a probe of alginate concentration and therefore of interstitial water content within the gel mesh. Changes in water proton relaxation may also reflect conformational changes, variation in gel rigidity (T_{2gel}) and/or in the proton exchange rate (k_{gel}) due to variations in pH. Our results suggest that polymer concentration is not constant across the beads rather it is higher at the edge compared to the centre. This is more marked in the strong beads at control conditions although both strong and weak bead systems display this phenomenon in gastric conditions following shrinkage.

We have shown changes in the alginate gel network following GI incubation for both bead types. In gastric conditions, the beads shrink due to a decrease in the electrostatic repulsive charge between alginate chains following protonation of free carboxyl groups. Furthermore, at low pH, the calcium ions bound between alginate chains may become dissociated and replaced with hydrogen ions, allowing the chains to move closer together as a result of hydrogen bonding and the formation of an "acid" gel (Norton, Frith, & Ablett, 2006). T_2 was also observed to shorten in gastric conditions presumably as a result of water loss and increased concentration of the alginate polymer within the gel beads on shrinkage. This corroborates our previous results obtained during swelling and T_2 experiments where these systems shrank by approximately 50% and T_2 decreased in the gastric phase, respectively (Rayment et al., 2009).

In intestinal conditions, both bead types swelled presumably due to an increase in the electrostatic repulsive forces at a pH above the pK_a of the uronic acid groups on the alginate. Furthermore, we show that the MR image intensity and T_2 increase for both bead type and becomes more homogeneous across the bead

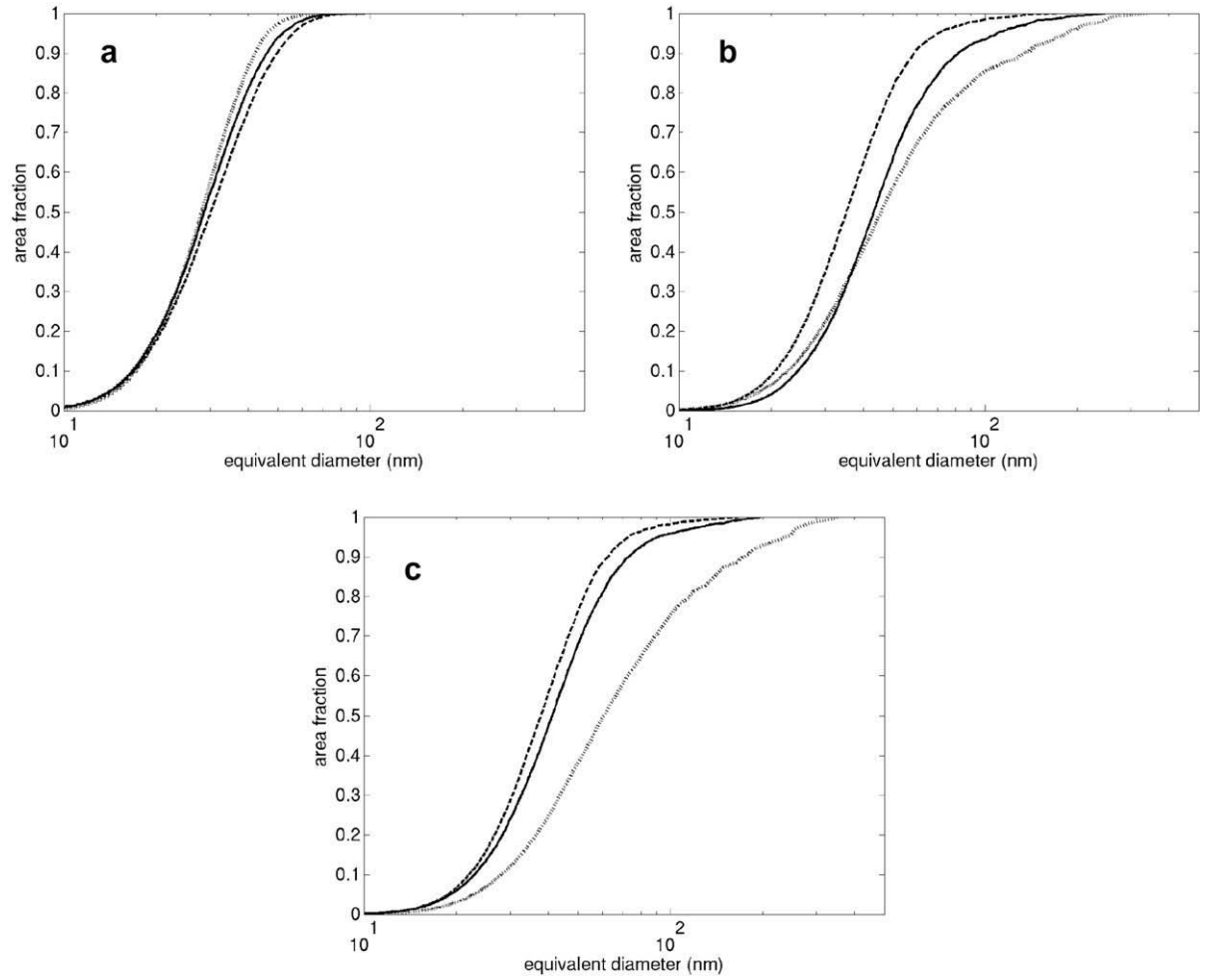

Fig. 10. Watershed analysis of TEMs of strong alginate gel bead at (a) edge (outside) (b) halfway-in (middle) and (c) centre (inside) in control (solid line), gastric (dashed line) and intestinal conditions (dotted line, appears almost grey).

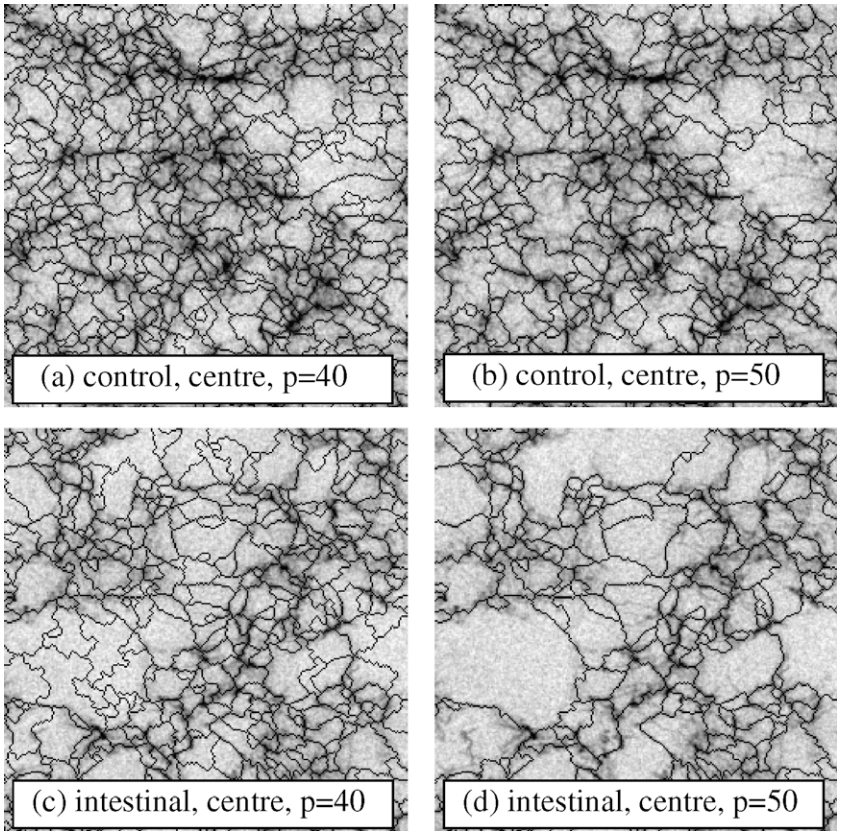

Fig. 11. The watershed contrast parameter is normally set to 40 and works well for most images. (a and b) In control conditions $p = 40$ represents the structure better than $p = 50$. (c and d) Under intestinal conditions there are larger pores more prone to oversegmentation (c). This can be resolved by increasing p to 50 (d).

diameter. We suggest this is due to solubilisation of the alginate gel at higher pH and monovalent ion concentration. In our previous work, the gel strength of the beads was reported and, during the intestinal phase, the Young's modulus of the strong and weak beads was not statistically different (Rayment et al., 2009) reflecting the increased swelling of the strong beads in this phase. Interestingly these changes appear to be independent of the method of bead manufacture. This should be taken into account when contemplating the use of such bead systems for potential applications such as encapsulation or controlled delivery. The time-resolved 3 T MRI data indicate that the major changes identified in gastric and intestinal conditions occur on a biologically relevant timescale and therefore suggests we may be able to use such techniques to determine similar changes in the beads *in vivo* within the human GI tract.

From our TEM results, and subsequent watershed image analysis, the majority of the changes appear to occur towards the centre of the bead rather than the outer edge. Here, the gel network remains denser throughout the GI incubation. We observed that the outer "skin" of the bead is more robust than the gel network at the centre of the bead, holding the bead intact until it eventually disintegrates in the intestinal phase where the whole bead falls apart. This is probably due to the higher alginate concentration at the edge of the bead which provides the bead with a strong, outer layer which takes longer to solubilise in intestinal conditions.

The watershed image analysis tool has proved a useful technique to quantify changes in alginate gel porosity following bead manufacture and GI incubation. A greater proportion of larger pores are found at the centre of the bead compared to the edge and similarly following intestinal incubation. These results complement our findings using both spatially resolved NMR and TEM techniques.

5. Conclusions

Alginate beads prepared using an external diffusion method have been characterised using MRI and TEM techniques. Our results suggest there is an inhomogeneous distribution of alginate polymer concentration across the beads with a higher concentration at the edge compared to the centre. This inhomogeneity has been shown to persist following incubation in simulated GI conditions. In particular, the denser gel microstructure at the edge of the beads remains unchanged despite the expansion and eventual disintegration of the gel at the centre of the beads towards the end of the intestinal phase. The changes in gel porosity have been demonstrated using transmission electron microscopy and have been shown to be dependant on both gel location and the chemical stimuli provided by the simulated GI conditions. Gel porosity has been quantified using image analysis showing that the beads have a greater distribution of larger pores at the centre of the beads compared to the edge and in intestinal conditions compared to control and gastric conditions.

Our results have shown that MRI and TEM techniques can be used to characterise biopolymer gel networks such as alginate providing information regarding the changes in microstructure (e.g. polymer concentration, porosity) following manufacture and simulated GI incubation. We suggest that such changes in porosity of these alginate beads during simulated GI conditions may make these an attractive option for controlled delivery applications *in vivo*. Furthermore, by undertaking MRI at two different field strengths, we have been able to access both high spatial resolution, microstructural information at 7 T in simulated GI conditions as well as determine similar dynamic changes using a whole-body MRI scanner at 3 T which can be utilised to investigate the

behaviour of these physiologically responsive hydrogels within the GI tract of humans. On the basis of these findings, future work will extend this to probe gel microstructural changes *in situ* during GI transit using whole-body MRI.

Acknowledgement

The authors thank Unilever for permission to publish our results.

References

Ablett, S., Lillford, P. J., Baghdadi, S. M. A., & Derbyshire, W. (1976). NMR relaxation in polysaccharide gels and films. *American Chemical Society Symposium Series, 34*, 344–359.

Altman, P. L. (1961). In Dorothy S. Dittmer (Ed.), *Blood and other body fluids, analysis and compilation* (xvii, 539 pp 181). Washington, DC: Federation of American Societies for Experimental Biology.

Deichmann, R., Adolf, H., Noth, U., Morrissey, S., Schwarzbauer, C., & Haase, A. (1995). Fast T2-mapping with snapshot flash imaging. *Magnetic Resonance Imaging, 13*, 633–639.

Duez, J.-M., Mestdagh, M., Demeure, R., Goudemant, J. F., Hills, B. P., & Godward, J. (2000). NMR studies of calcium-induced alginate gelation. Part I. MRI tests of gelation models. *Magnetic Resonance in Chemistry, 38*, 324–330.

Emmerichs, N., Wingender, J., Flemming, H.-C., & Mayer, C. (2004). Interaction between alginates and manganese cations: Identification of preferred cation binding sites. *International Journal of Biological Macromolecules, 34*, 73–79.

Grant, G. T., Morris, E. R., Rees, D. A., Smith, P. J. C., & Thom, D. (1973). Biological interactions between polysaccharides and divalent cations: The egg-box model. *FEBS Letters, 32*, 195–198.

Green, D. W., Leveque, I., Walsh, D., Howard, D., Yang, X., Partridge, K., et al. (2005). Biomineralised polysaccharide capsules for encapsulation, organization, and delivery of human cell types and growth factors. *Advanced Functional Materials, 15*, 917–923.

Haug, A. (1961). The Affinity of some divalent metals to different types of alginate. *Acta Chemica Scandinavica, 15*, 1794–1795.

Haug, A., & Smidsrød, O. (1970). Selectivity of some anionic polymers for divalent metal ions. *Acta Chemica Scandinavica, 24*, 843–854.

Hills, B. P., Cano, C., & Belton, P. S. (1991). Proton NMR relaxation studies of aqueous polysaccharide systems. *Macromolecules, 24*, 2944–2950.

Hills, B. P., Godward, J., Debatty, M., Barras, L., Saturio, C. P., & Ouwerx, C. (2000). NMR studies of calcium induced alginate gelation. Part II. The internal bead structure. *Magnetic Resonance in Chemistry, 38*(9), 719–728.

Hoad, C., Rayment, P., Cox, E., Wright, P., Butler, M., Spiller, R., et al. (2009). Investigation of alginate beads for gastro-intestinal functionality, Part 2: In vivo characterisation. *Food Hydrocolloids, 23*, 833–839.

Kim, H.-S. (1990). A kinetic study on calcium alginate bead formation. *Korean Journal of Chemical Engineering, 7*(1), 1–6.

Luengo Hendriks, C. L., Rieger, B., van Ginkel, M., van Kempen, G. M. P. van Vliet, L. J. (1999). DIPimage: a scientific image processing toolbox for MATLAB, Delft University of Technology. Available from http://www.diplib.org.

Martinsen, A., Skjåk-Bræk, G., & Smidsrød, O. (1989). Alginate as immobilization material: I. Correlation between chemical and physical properties of alginate gel beads. *Biotechnology and Bioengineering, 33*, 79–89.

McKenzie, C. A., Chen, Z. Q., Drost, D. J., & Prato, F. S. (1999). Fast acquisition of quantitative T-2 maps. *Magnetic Resonance in Medicine, 41*, 208–212.

Mørch, Y. A., Donati, I., Strand, B. L., & Skjåk-Bræk, G. (2006). Effect of Ca^{2+}, Ba^{2+}, and Sr^{2+} on alginate microbeads. *Biomacromolecules, 7*, 1471–1480.

Norton, I. T., Frith, W. J., & Ablett, S. (2006). Fluid gels, mixed fluid gels and satiety. *Food Hydrocolloids, 20*(2–3), 229–239.

Ouwerx, C., Velings, N., Mestdaugh, M. M., & Axelos, M. A. V. (1998). Physico-chemical properties and rheology of alginate gel beads formed with various divalent cations. *Polymer Gels and Networks, 6*, 393–408.

Peppas, N. (2004). Kinetics of smart hydrogels. In N. Yui, R. Mrsny, & K. Park (Eds.), *Reflexive polymers and hydrogels: Understanding and designing fast-responsive polymeric systems* (pp. 99–113). Boca Raton, FL: CRC Press.

Potter, K., Carpenter, T. A., & Hall, L. D. (1993). Mapping of the spatial variation in alginate concentration in calcium alginate gels by magnetic-resonance-imaging (MRI). *Carbohydrate Research, 246*, 43–49.

Potter, K., Herrod, N. J., Carpenter, T. A., & Hall, L. D. (1993). Visualisation of the geometries of objects fabricated from calcium alginate, using magnetic resonance imaging. *Carbohydrate Research, 239*, 249–256.

Rayment, P., Wright, P. J., Hoad, C. L., Ciampi, E., Haydock, D., & Gowland, P. A (2009). Investigation of alginate beads for gastro-intestinal functionality, Part 1. In vitro characterisation. *Food Hydrocolloids, 23*, 816–822.

Simpson, N. E., Grant, S. C., Blackband, S. J., & Constantinidis, I. (2003). NMR properties of alginate microbeads. *Biomaterials, 24*, 4941–4948.

Skjåk-Bræk, G., & Espevik, T. (1996). Application of alginate gels in biotechnology and biomedicine. *Carbohydrates in Europe: Challenges in Alginate Research, 14*, 6–13.

Skjåk-Bræk, G., Grasdalen, H., & Smidsrød, O. (1989). Inhomogeneous polysaccharide ionic gels. *Carbohydrate Polymers, 10*, 31–54.

Smidsrød, O. (1974). Molecular basis for some physical properties of alginates in the gel state. *Journal of the Chemical Society Faraday Transactions, 57*, 263–274.

Smidsrød, O., & Draget, K. I. (1996). Chemistry and physical properties of alginates. *Carbohydrates in Europe: Challenges in Alginate Research, 14*, 6–13.

Soille, P. (1999). *Morphological image analysis principles and applications*. Springer-Verlag.

Strand, B. L., Mørch, Y. A., Espevik, T., & Skjåk-Bræk, G. (2003). Visualization of alginate-poly-L-lysine-alginate microcapsules by confocal laser scanning microscopy. *Biotechnology and Bioengineering, 82*(4), 386–394.

Thu, B., Bruheim, P., Espevik, T., Smidsrød, O., Soon-Shiong, P., & Skjåk-Bræk, G. (1996). Alginate polycation microcapsules. II Some functional properties. *Biomaterials, 17*, 1069–1079.

Thu, B., Gaserod, O., Paus, D., Mikkelsen, A., Skjåk-Bræk, G., & Toffanin, R. (2000). Inhomogenous alginate gel spheres: An assessment of polymer gradients by synchrotron radiation-induced X-ray emission, magnetic resonance micro-imaging, and mathematical modelling. *Biopolymer, 53*, 60–71.

Tønnesen, H. H., & Karlsen, J. (2002). Alginate in drug delivery systems. *Drug Development and Industrial Pharmacy, 28*(6), 621–630.

Tyler, D. J., Moore, R., Marciani, L., & Gowland, P. A. (2004). Rapid and accurate measurement of transverse relaxation times using a single shot multi-echo echo-planar imaging sequence. *Magnetic Resonance Imaging, 22*, 1031–1037.